5 (2025) 100047

Contents lists available at ScienceDirect

Materials Chemistry and Physics: Sustainability and Energy

journal homepage: www.sciencedirect.com/journal/materials-chemistry-and-physics-sustainability-and-energy

Innovative asymmetric supercapacitor cell design: Harnessing CuS and WO3 for enhanced energy storage

Irem Ertugrul [a], Fatma Kilic Dokan [b,*], Nuri Burak Kiremitler [a,c], Mustafa Serdar Onses [a,c,d], Ertugrul Sahmetlioglu [e,**]

[a] ERNAM-Erciyes University Nanotechnology Application and Research Center, Kayseri, 38039, Turkey
[b] Department of Chemistry and Chemical Processing Technologies, Mustafa Çıkrıkcıoglu Vocational School, Kayseri University, Kayseri, Turkey
[c] Department of Materials Science and Engineering, Faculty of Engineering, Erciyes University, Kayseri, 38039, Turkey
[d] UNAM–Institute of Materials Science and Nanotechnology, Bilkent University, Ankara, 06800, Turkey
[e] Department of Basic Sciences of Engineering, Kayseri University, Kayseri, 38039, Turkey

A B S T R A C T

In today's world, the pressing issues of environmental pollution and the need for advanced energy storage systems are at the forefront of scientific research. Addressing these challenges is vital for ensuring a sustainable and cleaner future. These environmental concerns, coupled with the ever-growing demand for efficient energy storage, call for innovative solutions to meet global energy needs while minimizing ecological impacts.

This study explores a promising approach to these problems by focusing on the development of high-performance energy storage devices. Specifically, we synthesized copper sulfide (CuS) using a hydrothermal method to create the cathode material and tungsten oxide (WO_3), a transition metal oxide, using the same method for the anode. The synthesis of both materials through hydrothermal processing is advantageous as it allows for the creation of high-purity and well-structured compounds suitable for energy storage applications.

The resulting supercapacitor device demonstrates impressive electrochemical properties, achieving a high specific capacitance of 211.43 F/g, which reflects its ability to store a large amount of charge per unit mass. This is further complemented by an excellent energy density of 247.6 Wh kg^{-1}, indicating the device's capacity to store substantial energy relative to its weight. Additionally, it boasts a high-power density of 1.451 kW kg−1 at a current density of 1 A g−1, highlighting its potential for rapid discharge and efficient energy delivery when needed.

1. Introduction

Energy storage innovations are crucial for driving economic expansion and societal progress. Supercapacitors (SCs) are compelling energy storage solutions known for their exceptional features, including rapid charge and discharge rates, impressive power density, and extended operational lifespan [1,2].

Supercapacitors stand out for their unique combination of features that make them superior to conventional batteries in certain contexts. One of the most notable advantages is their rapid charge and discharge rates. Unlike traditional batteries, which typically require a considerable amount of time to recharge, supercapacitors can absorb and release energy almost instantaneously, making them ideal for applications that require quick bursts of power. This is particularly advantageous in sectors like electric vehicles, grid stabilization, and portable electronics, where rapid energy delivery and replenishment are essential [3].

Another key feature of supercapacitors is their impressive power density. Power density refers to the amount of energy that can be delivered per unit of time, and SCs excel in this area, providing high bursts of power for short durations. This property is crucial in applications that demand high-power outputs, such as regenerative braking systems in electric vehicles or pulse power applications in various industrial processes [4]. Moreover, supercapacitors are known for their long operational lifespan compared to other energy storage devices. While conventional batteries degrade over time, losing their ability to hold a charge, supercapacitors experience minimal wear and tear and can operate for hundreds of thousands or even millions of charge-discharge cycles. This durability significantly reduces the need for frequent replacements, lowering maintenance expenses and contributing to a more sustainable energy infrastructure. Supercapacitors also offer high efficiency, with minimal energy loss during the charge and discharge process, which leads to a lower overall environmental footprint. This makes them an excellent option for integrating renewable energy sources, where energy fluctuations can be balanced

* Corresponding author.
** Corresponding author.
E-mail addresses: irem771881@gmail.com (I. Ertugrul), fatmakilic@kayseri.edu.tr (F.K. Dokan), sahmetlioğlu@kayseri.edu.tr (E. Sahmetlioglu).

https://doi.org/10.1016/j.macse.2025.100047
Received 27 February 2025; Received in revised form 9 October 2025; Accepted 10 October 2025
Available online 25 October 2025
3050-4716/© 2025 Elsevier B.V. All rights are reserved, including those for text and data mining, AI training, and similar technologies.

with the rapid storage and retrieval capabilities of SCs. However, despite their impressive attributes, supercapacitors are limited by their relatively low-energy density compared to conventional batteries, which restricts their ability to store large amounts of energy for long periods. As a result, ongoing research and innovation are focused on enhancing the energy storage capacity of SCs while maintaining their fast charge-discharge rates and long cycle life. Based on various energy storage techniques, supercapacitors can be categorized into two types: electrochemical double-layer capacitors (EDLCs) and pseudocapacitors [5]. The charge storage in EDLCs occurs through ion absorption at the interface between the electrode and the electrolyte. Typically constructed from carbon-based materials with high surface areas, EDLCs offer excellent charge and discharge capabilities. However, their specific capacitance remains relatively low, ranging from 10 F/g to 200 F/g [6]. In contrast to EDLCs, pseudocapacitors store electrical charge through both physical mechanisms and faradaic processes. These faradaic processes involve rapid and reversible redox reactions occurring on or near the surface of the electrode's active materials, enhancing the charge storage capability [7].

Transition metal sulfides (TMS) have garnered considerable interest in recent years as a result of their exceptional electrochemical properties, making them highly promising materials for a broad spectrum of energy storage and conversion applications. These materials are gaining popularity as alternatives to traditional electrode materials due to their unique characteristics that enhance the performance of various energy storage devices, such as supercapacitors, batteries, and even fuel cells. TMS are particularly valued for their ability to provide both high-energy and power densities, crucial factors for the development of more efficient and sustainable energy storage systems [8,9].

One of the most remarkable properties of TMS is their high electrical conductivity, which significantly enhances the efficiency of electron transport during electrochemical reactions. This conductivity facilitates smoother and faster electron movement within the material, leading to improved charge and discharge rates. The ability to efficiently transport electrons is vital for energy storage devices, as it directly impacts their power density and overall operational speed. In the context of supercapacitors, for instance, the rapid electron flow allows for quick charge and discharge cycles, which is essential for applications requiring bursts of energy in a short period of time, such as electric vehicles, portable electronics, and grid stabilization.

Additionally, the high electrical conductivity of TMS contributes to reducing the internal resistance of energy storage devices, further optimizing their performance. This lower resistance results in enhanced efficiency and improved energy storage capabilities. It also plays a crucial role in minimizing heat generation during charge and discharge cycles, which is a common issue in other types of energy storage systems, particularly batteries. By mitigating these issues, TMS-based devices can operate more efficiently and with greater longevity, making them ideal for sustainable and long-lasting energy solutions.

Beyond electrical conductivity, transition metal sulfides also exhibit high theoretical capacitance and large surface areas, which are beneficial for energy storage. These properties enable TMS to store more charge, further enhancing their energy storage capacity. The combination of good conductivity and high charge storage potential makes TMS ideal candidates for use in both supercapacitors and batteries, where both power and energy density are critical parameters. For instance, in supercapacitors, TMS can serve as electrodes that provide rapid charge/discharge cycles while also storing substantial amounts of energy. In batteries, their stable electrochemical behavior and high capacity can translate into longer-lasting energy storage systems.

Furthermore, the synthesis of TMS materials can be tailored to optimize their performance for specific applications. By adjusting factors such as particle size, morphology, and composition, researchers can fine-tune the electrochemical properties of TMS to meet the demands of particular energy storage technologies. For example, doping transition metal sulfides with other elements or composites can enhance their electrochemical stability, cycling life, and overall efficiency [10]. Transition metal sulfides also offer advantages in terms of environmental sustainability and cost-effectiveness. Many transition metals used in TMS are abundant and inexpensive, which contrasts with the scarcity and high cost of some materials used in conventional energy storage devices, such as lithium. This makes TMS a more economically viable and environmentally friendly alternative for large-scale energy storage solutions, especially in applications like renewable energy storage, where cost and sustainability are of paramount importance [10]. Furthermore, TMS has been found to have a higher specific capacity compared to traditional electrode materials, allowing them to store a higher amount of energy per unit mass. This higher capacity contributes to increased energy density in devices, making TMS an attractive option for next-generation energy storage solutions. These properties combined make transition metal sulfides an important player in the development of advanced materials for sustainable energy technologies. [11,12]. Examples of transition metals such as NiS [13], MoS_2 [14], and CuS [15], which are most commonly used in energy storage systems, can be given. For example, Huang et al. synthesized a CuS@MWCNT hybrid structure via a facile hydrothermal method process. The resulting composite combines the benefits of CuS and CNT with specific capacitance of 2831.0 F/g at 1 A g^{-1} current density [16].

Since transition-metal oxides have rich electrochemistry and provide better specific capacitance and energy density, they have been extensively researched as supercapacitor electrode materials [17]. Because of its exceptional electrochemical qualities, including strong proton conductivity and a highly reversible redox process, RuO_2 has been the subject of extensive investigation among metal oxides [18]. However, the use of RuO_2 is limited due to its toxicity and high cost [19]. It therefore compels us to search for substitutes, like MnO_2 [20], NiO [21], and WO_3 [22]. For example, Saini et al. synthesized the tungsten oxide (WO3) metal oxide structure using a straightforward hydrothermal method combined with a calcination process. This approach is advantageous as it allows for the controlled fabrication of high-purity WO_3 with well-defined microstructures, which can significantly enhance its electrochemical properties. The hydrothermal method, in particular, facilitates the formation of nanostructured materials that exhibit improved surface areas and better charge storage capacities, while the calcination step ensures the material's crystallinity and stability, essential for long-term performance in energy storage applications [23–26].

The resulting WO_3 exhibited a remarkable specific capacitance of 741 F/g at a current density of 1 mA. This value is particularly impressive as it reflects the material's high efficiency in storing and delivering charge during electrochemical reactions. A specific capacitance of 741 F/g indicates that the WO_3 material is capable of storing a large amount of electrical charge relative to its mass, which is a crucial attribute for supercapacitors and other energy storage devices. The ability to achieve such high capacitance is a testament to the superior electrochemical properties of the synthesized WO_3, which are likely due to its optimal structural configuration and enhanced surface area. Moreover, the high specific capacitance of WO_3 at low current densities, like the 1 mA used in the study, suggests that the material is well-suited for applications requiring stable and reliable energy storage over extended periods. This is particularly beneficial for supercapacitors, where maintaining high capacitance at varying current densities is important for ensuring performance under different operating conditions. WO_3's ability to deliver substantial capacitance while maintaining stability further enhances its potential for use in energy storage systems, especially those integrated with renewable energy sources, where the rapid charge-discharge capability is a key requirement. The synthesis method used in this study also highlights the significance of combining hydrothermal techniques with post-synthesis treatments, such as calcination, to fine-tune the material's properties for optimal performance. This dual approach allows for better control over the material's morphology, phase composition, and conductivity, resulting in an

electrochemical behavior that is well-suited for high-performance energy storage devices. In summary, the work by Saini et al. demonstrates the successful synthesis of WO_3 through a hydrothermal and calcination process, yielding a material with excellent electrochemical performance, including a high specific capacitance of 741 F/g at 1 mA. This outcome underscores the potential of WO_3 and similar transition metal oxides as effective materials for supercapacitors and other energy storage applications, offering a pathway to more efficient and durable energy storage technologies [26].

In this study, we present the design of a novel asymmetric supercapacitor constructed using **copper sulfide (CuS)** as the cathodic material and **tungsten oxide (WO_3)** as the anodic counterpart. Both electrode materials were synthesized via a straightforward yet efficient **hydrothermal method**, which offers precise control over morphology, crystallinity, and purity critical factors for optimizing electrochemical performance. The strategic pairing of CuS and WO_3 takes advantage of their **complementary electrochemical characteristics**: CuS, with its high electrical conductivity and large surface area, enables rapid charge accumulation, while WO_3 contributes excellent electrochemical stability and high capacitance due to its multiple oxidation states. This synergistic configuration not only broadens the operating voltage window but also significantly boosts both energy and power density. As a result, the device exhibits fast charge–discharge capabilities, making it a **promising solution for next-generation energy storage systems** where both efficiency and durability are essential.At a current density of 1 A g^{-1}, the asymmetric supercapacitor developed in this study demonstrates an impressive energy density of 247.6 Wh kg^{-1} and a power density of 1.451 kW/kg. These values reflect a remarkable balance between energy storage and power delivery capabilities two critical parameters for the practical deployment of supercapacitors in modern energy systems. An energy density of 247.6 Wh kg^{-1} signifies the device's ability to store a substantial amount of energy relative to its mass, while a power density of 1.451 kW/kg highlights its capacity to release energy rapidly when required. This synergistic performance is essential for applications such as electric vehicles, portable electronics, and grid stabilization, where both high energy retention and instantaneous power delivery are paramount.

The superior performance of the device is largely attributed to its asymmetric configuration, which utilizes electrode materials with distinct electrochemical characteristics. This design enables a broader operating voltage window compared to symmetric counterparts, directly contributing to the enhanced energy density. Furthermore, the hydrothermal synthesis method employed in fabricating the electrode materials is not only simple and environmentally friendly but also highly scalable, offering significant advantages for future industrial-scale production. The findings of this work underscore the potential of asymmetric supercapacitor architectures in addressing the growing demand for efficient, high-performance, and cost-effective energy storage Technologies [28].

2. Experimental Section

2.1. Materials

Copper nitrate trihydrate (Cu $(NO_3)_2.3H_2O$) and n-methyl 2-pyrrolidone (NMP) provided by Merck. Polyvinylidene fluoride (PVDF) and thiourea (CH_4N_2S) were obtained from Sigma Aldrich. Sodium tungstate dihydrate ($Na_2WO_4.2H_2O$) was supplied by Acros. Sodium chloride (NaCl) was obtained from Galenik.

2.2. Synthesis of CuS

A green solution was generated after dissolving 0.9964 g of copper nitrate trihydrate (Cu $(NO_3)_2{\cdot}3H_2O$) in 40 mL of water. Subsequently, 0.91 g of thiourea (CH_4N_2S) were included in the mixture. The final step was moving the resultant solution into an autoclave. Within a stainless-steel tank, the autoclave was sealed and maintained at 150 °C for a duration of 15 h. After allowing the autoclave to cool to ambient temperature, the black materials that emerged were centrifuged at 4000 rpm and repeatedly cleaned with distilled water and 100 % ethanol. The items were then dried for 2 h at 100 °C [27].

2.3. Synthesis of WO_3

Synthesis of Tungsten Oxide (WO_3),Tungsten oxide (WO_3) was synthesized using a previously documented hydrothermal method. The synthesis procedure began by dissolving 0.935 g of sodium chloride (NaCl) and 1.056 g of sodium tungstate dihydrate ($Na_2WO_4{\cdot}2H_2O$) in 30 ml of deionized (DI) water. The solution was stirred for 20 min to ensure complete dissolution of the salts. Afterward, 3 M hydrochloric acid (HCl) was gradually added to the solution until the pH reached 2, and the mixture was stirred for an additional 3 h to ensure thorough mixing and adjustment of the pH.Once the solution was prepared, it was transferred into a Teflon-lined autoclave for the hydrothermal reaction. The autoclave was sealed, and the solution was heated to 180 °C and maintained at this temperature for 24 h to allow the formation of tungsten oxide (WO_3) through the hydrothermal process. The high temperature and pressure inside the autoclave facilitated the synthesis of WO_3 with a controlled morphology and structure.

After the reaction, the product was thoroughly washed multiple times with DI water to remove any residual impurities or by-products. The resulting WO_3 was then dried at 60 °C to obtain a fine, powdery form of the material, ready for further characterization and application in energy storage devices.This hydrothermal synthesis method, coupled with the subsequent cleaning and drying steps, ensured the formation of high-purity WO_3 with optimal structural and electrochemical properties for use in energy storage applications, particularly in supercapacitors and other advanced energy devices [29].

2.4. Preparation of electrodes and electrochemical testing

GAMRY Reference 3000 potentiostat was used to examine the electrodes' electrochemical activity at room temperature. Electrodes obtained by different methods with the nanoparticles produced were used as working electrodes, the Ag/AgCl electrode as a reference electrode, and platinum foil as a counter electrode, and a three-electrode arrangement was created. To make an electrode from the synthesized CuS nanoparticles, they were deposited on Ni foam using the hydrothermal method. 0.05 g of the synthesized CuS was mixed with 20 ml of water, cleaned with 1M HCl, and placed in a Teflon autoclave along with Ni foam with an area of 1.1 cm diameter and kept at 120° for 10 h. The produced active material WO_3 was mixed with acetylene black (10 wt %), polyvinylidene fluoride (5 wt%), methyl-2-pyrrolidone (NMP), and active material (85 wt %) to form a mixture and sonicated for 1 h. After applying the slurry to the nickel foam, it was vacuum-dried at 80° for 12 h. In the study, the amount of substance in the CuS electrode to be used as the cathode was about 2 mg, while the amount of the substance in the WO_3 electrode to be used as the anode was about 1 mg. Electrochemical measurements were made using 2M KOH electrolyte. The low active material masses used for electrode fabrication (1mgfor theWO3 anode and2mgfor the CuS cathode) were specifically chosen to maximize the accuracy and repeatability of our electrochemical measurements. This scale allows us to more effectively investigate the intrinsic properties of the materials by minimizing external factors such as contact resistance or ion transport limitations that can be prevalent in larger-scale devices. To ensure the reliability of our data at this small scale, all materials were weighed with a high-precision microbalance (±0.01 mg), and the slurry was thoroughly sonicated to achieve a homogeneous mixture before casting.

From the discharge curves of the galvanostatic study, the specific capacitances of the electrodes were determined as follows:

$$C = \frac{I \times \Delta t}{m \times \Delta V} \quad (1)$$

The discharge current, discharge time, active material mass, and potential window during the discharge were denoted by the values I, Δt, m, and ΔV, respectively. Equation (1) was utilized to compute the specific capacitances of the ASc, whereby m represents the total mass of the two electrodes. Based on galvanostatic charge-discharge (GCD) analysis, the supercapacitors' energy density (E) and power density (P) were subsequently determined using the following formulas:

$$E(Wh/kg) = \frac{C \times (\Delta V)^2}{2 \times 3.6} \quad (2)$$

$$P(W/kg) = \frac{3600 \times E}{\Delta t} \quad (3)$$

The frequency range for the electrochemical impedance spectroscopy (EIS) was 10 kHz to 0.01 Hz.

3. Results and discussion

Various characterization techniques were employed to clarify the structure of the synthesized materials. Fig. 1a and b shows the XRD pattern of CuS and WO_3. XRD measurements were made, and the JCPDS card number (00-006-0464) was compared. It is clear that the production of single-phase CuS powder was accomplished. The resulting CuS material appears to be well crystallized, based on the distinct diffraction peaks. It is evident from XRD patterns that all the diffraction peaks are well indexed to WO_3's hexagonal phase (JCPDS 33–1387) [30]. The crystal structure of the materials was characterized using X-ray diffraction (XRD) analysis, as shown in Fig. 1a. The characteristic XRD peaks for WO_3 (copper(I) sulfide) powder typically appear at specific 2θ angles. The most prominent peaks for Fig. 1 b CuS correspond to the following values: 27.5° (111), 32.5° (200), 39.5° (211), 45.5° (220), and 48.5° (311). Similarly, the characteristic XRD peaks for tungsten trioxide (WO_3) also appear at specific 2θ angles. For the most stable orthorhombic phase of WO_3, the peaks are as follows: 23.1° (110), 24.3° (200), 25.3° (111), 28.5° (210), 31.2° (220), 33.2° (112), 35.2° (301), and 38.1° (221).

Furthermore, the components contained in the resulting CuS and WO_3 materials were identified using energy dispersive spectroscopy (EDS). Copper and sulfur are observed in the composite structure as major elements in Fig. 2c. EDS indicated the Cu/S weight ratio in the composite as shown in Fig. 3d, which proves the existence of CuS elements. Major elements of WO_3 that are observed in the composite structure are tungsten and oxygen, as shown in Fig. 3b. The structure and morphology of the synthesized materials were characterized with FESEM images. Fig. 2a-b shows the presence of nanometer-sized particles and rod-like microsphere structures of WO_3. The FESEM image of CuS displays the rod-like shape in Fig. 2c-d.

In the FESEM images of CuS, the material often exhibits nanoparticles or nanoflakes, which are key to its high surface area and charge storage capacity. The high-resolution FESEM images can reveal the uniformity and size distribution of the nanoparticles, both of which are crucial for optimizing the electrochemical performance of CuS in supercapacitor applications [31]. The nanostructured morphology of CuS allows for an enhanced interface between the electrode and electrolyte, which facilitates better charge transfer and improves the overall efficiency of the energy storage device. The roughness and porosity visible in the FESEM images suggest that CuS may have a high surface-to-volume ratio, which is beneficial for increasing the active sites for electrochemical reactions. This morphology enhances its rate capability, meaning it can charge and discharge rapidly, which is a desirable property for high-performance energy storage systems. The EDS spectrum of both WO_3 and CuS provides quantitative data on the elemental composition of the materials, confirming the presence of tungsten (W) and oxygen (O) in WO_3 and copper (Cu) and sulfur (S) in CuS [28]. For WO_3, the EDS spectrum will show characteristic peaks for tungsten (W) and oxygen (O), confirming the successful synthesis of tungsten oxide. The relative intensities of these peaks can provide insight into the stoichiometry of the material, indicating whether the material is stoichiometrically balanced or if there are any deficiencies or excesses in the oxygen content. These features are important for understanding the electrochemical behavior of WO_3, especially its stability and performance during cycling in energy storage applications. For CuS, the EDS spectrum will display distinct peaks for copper (Cu) and sulfur (S), confirming the formation of copper sulfide. The intensity ratio between copper and sulfur peaks is important for verifying the purity of the material and ensuring that the Cu:S ratio is optimal for electrochemical applications [31].

In the EDX data, the elemental compositions of WO_3 and CuS were thoroughly analyzed to confirm the presence and distribution of the constituent elements. Fig. 3 presents the EDX spectra and elemental mapping images for WO_3 (Fig. 3a and b) and CuS (Fig. 3c and d), respectively. The elemental maps clearly demonstrate a uniform distribution of tungsten (W) and oxygen (O) within the WO_3 sample, as well as copper (Cu) and sulfur (S) within the CuS sample. These results confirm the successful synthesis of the targeted compounds with homogeneous elemental dispersion, which is essential for their anticipated electrochemical performance. The EDX analysis thus provides critical insight into the purity and compositional integrity of the synthesized

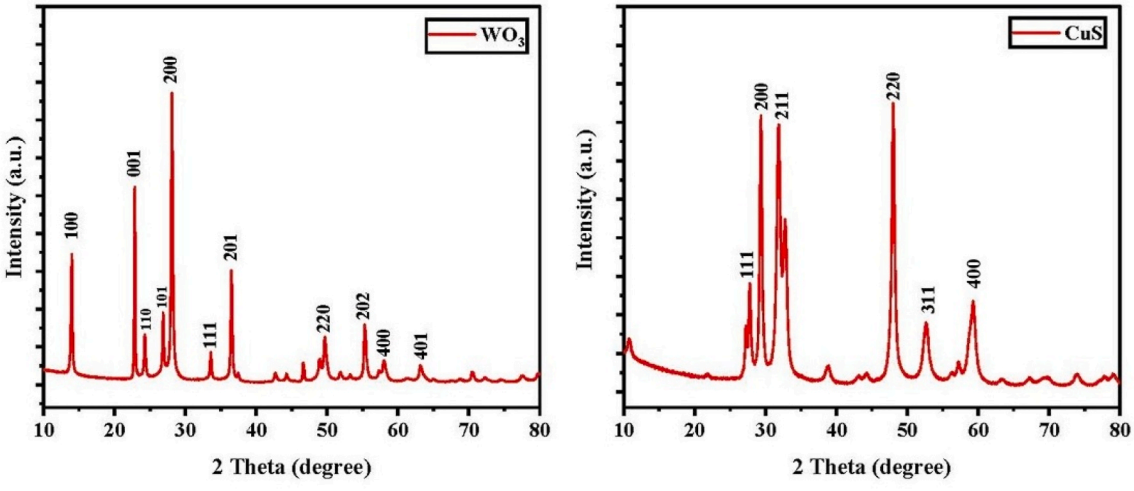


Fig. 1. X-ray diffraction pattern of a) CuS and b)WO_3 samples.

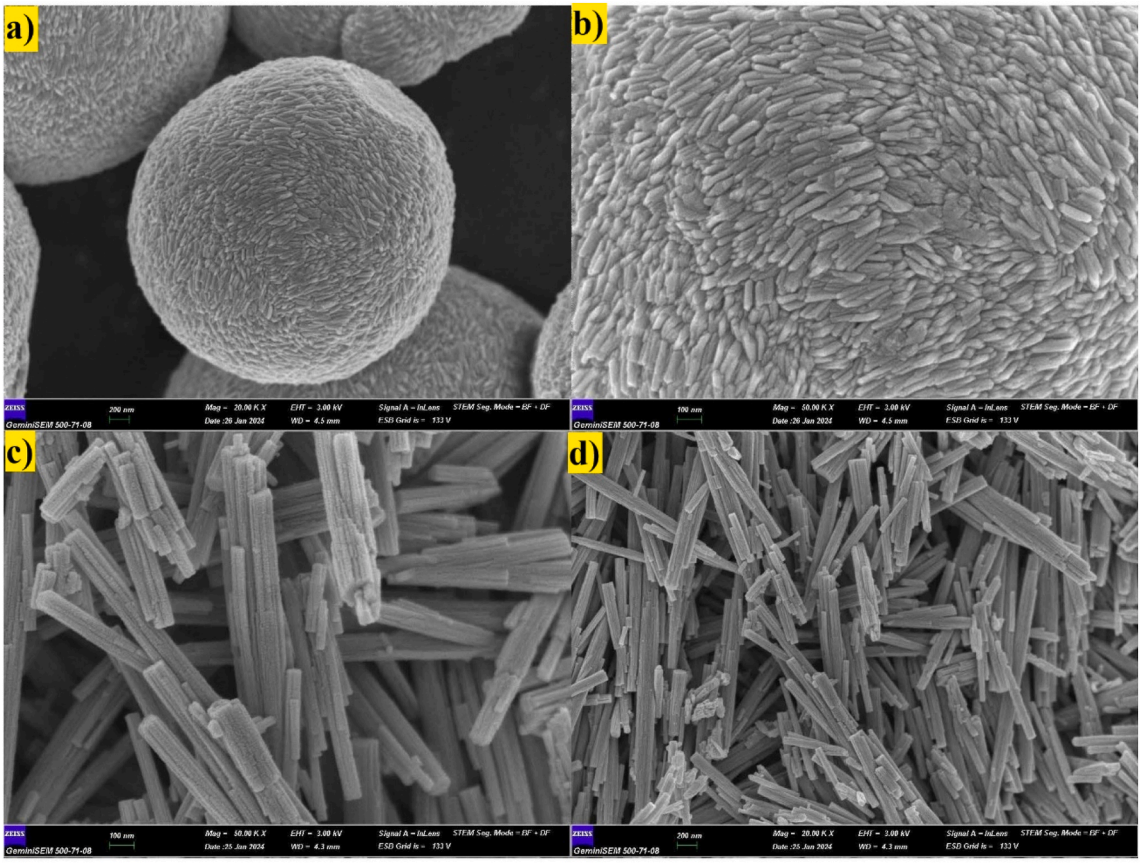


Fig. 2. Material characterization of CuS and WO_3; (a–b) FESEM images of WO_3; (c–d) FESEM images of CuS.

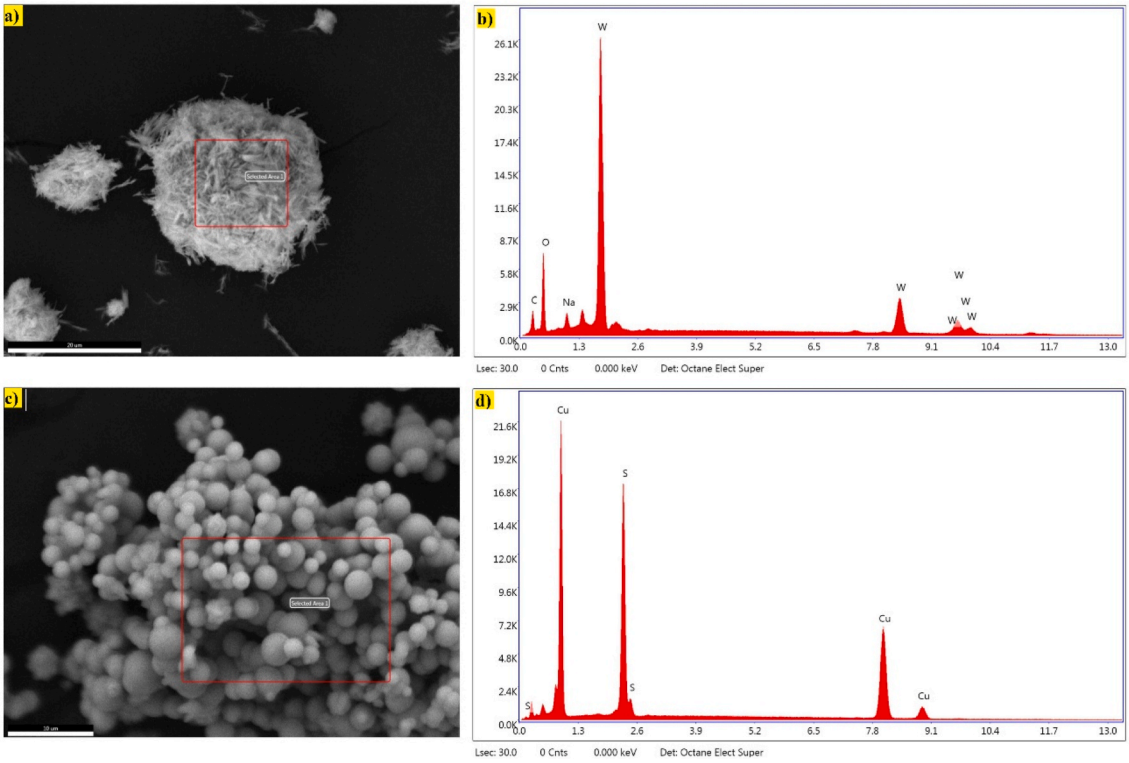


Fig. 3. EDX images and elementel mapping results of WO_3 (a–b); CuS (c–d).

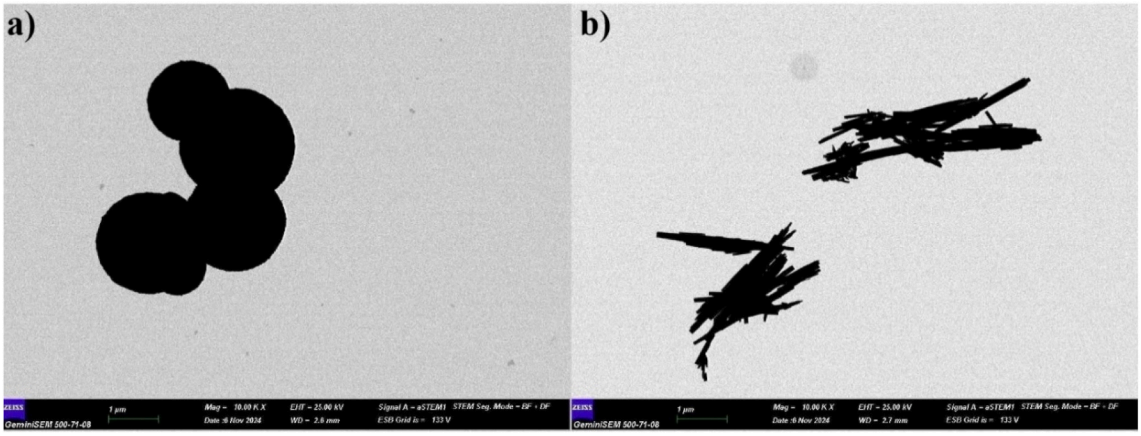


Fig. 4. STEM images of (a) WO_3; (b) CuS.

materials.

In STEM images of WO_3 (Fig. 4a), the material often exhibits well-defined nanostructures, which can range from nanoplates to nanorods, depending on the synthesis conditions. The high-resolution STEM images of WO_3 typically reveal well-ordered crystalline structures with a distinctive (001) plane orientation [32,33], which is important for the material's electrochemical behavior. The uniformity of the particle size and high crystallinity observed in the STEM images are crucial for improving the electrochemical stability and charge-discharge cycling performance of WO_3 when used in energy storage applications. The grain boundaries visible in the STEM images of WO_3 can act as sites for ion and electron transport, making them advantageous for charge storage. In addition, the porosity and surface area observed in WO_3 structures play a significant role in enhancing the material's specific capacitance and energy density [34–37]. For example, the mesoporous structure in WO_3 increases the effective surface area, facilitating better electrolyte interaction and higher charge storage. In STEM images of CuS, the material typically shows nanoparticles or nanoflakes with a high surface-to-volume ratio, which is beneficial for improving charge transfer kinetics. CuS's high electrical conductivity and well-defined surface structure can contribute to its superior performance in supercapacitors where efficient electron flow and high surface area are essential.

Fig. 5 shows the results of bet analyses for WO_3 and CuS. For CuS, nitrogen adsorption-desorption isotherms typically display a type IV isotherm according to the Brunauer-Emmett-Teller (BET) classification, which is indicative of materials with mesoporous structures. In such isotherms, an initial sharp increase in nitrogen adsorption occurs at low relative pressures (P/P_0), indicating the presence of micropores. As the relative pressure increases, the adsorption continues more gradually and eventually plateaus, which reflects the filling of mesopores [31]. This type of isotherm suggests that CuS possesses a combination of micropores and mesopores, both of which are beneficial for increasing the material's surface area and enhancing its charge storage capacity. The BET surface area is often calculated from the adsorption data in the low-pressure region, which corresponds to the monolayer adsorption of nitrogen molecules. For CuS, a high BET surface area is desirable because it provides more active sites for electrochemical reactions, thereby enhancing the overall performance in supercapacitors. For WO_3, the nitrogen adsorption-desorption isotherm generally shows a type IV isotherm as well, with the characteristic hysteresis loop observed in the adsorption-desorption curves. This is indicative of the mesoporous nature of WO_3. The hysteresis loop suggests that WO_3 has larger pores that can accommodate nitrogen molecules at higher relative pressures (P/P_0), and these pores are likely responsible for the rapid charge and discharge characteristics in supercapacitor applications [38]. The surface area of WO_3, typically calculated by the BET method, is also an important parameter. Higher surface area generally results in more available sites for electrochemical reactions, improving the specific capacitance of the material. The pore volume and pore size distribution are also important factors that influence the efficiency of charge storage and transfer within WO_3-based energy devices.

Both CuS and WO_3 benefit from their mesoporous structures, as they provide a high surface area that is beneficial for electrochemical

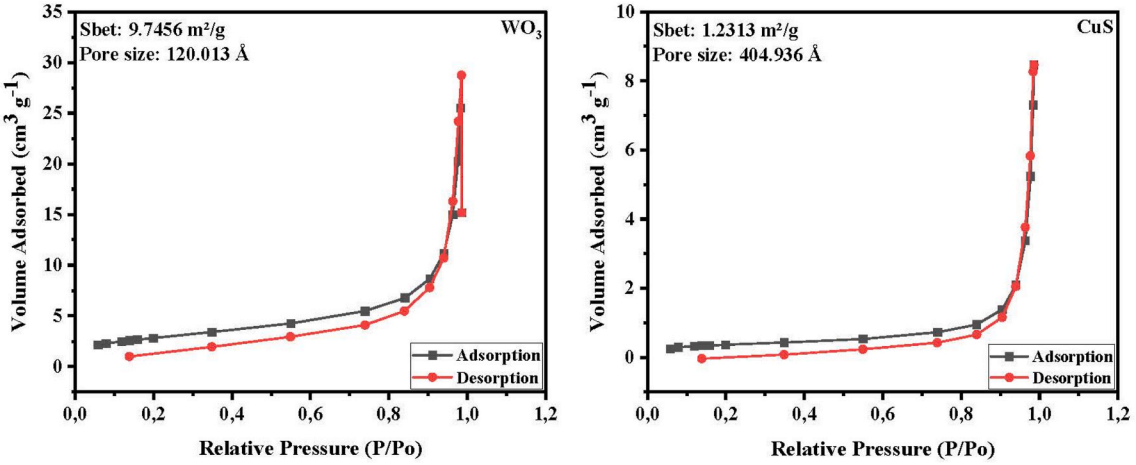


Fig. 5. Nitrogen adsorption-desorption isotherm for CuS and WO_3.

performance. CuS, with its high conductivity and mesoporous nature, is highly effective at enhancing the charge transfer process, making it a suitable material for supercapacitors. WO_3, with its stable electrochemical properties and high surface area, offers excellent charge storage capacity, particularly in asymmetric supercapacitor designs. The nitrogen adsorption-desorption isotherms for both materials indicate that they are well-suited for use in energy storage devices due to their ability to store significant amounts of charge and deliver high-power densities [34].

3.1. Electrochemical measurements

The capacitive performance of the CuS electrode was evaluated by using a 2 M KOH aqueous solution as the electrolyte in a three-electrode system. Cyclic voltammetry is a technique for determining whether or not an electrode material has capacitive properties [38]. The cyclic voltammetry (CV) of the CuS electrode was assessed within the potential range of −0.2–0.7 V at a scan rate in the range of 5–100 mV/s. The CV curves in Fig. 6a indicate a pair of broad and clear redox peaks, which relate to the characteristic faradaic reactions. The anodic and cathodic peaks show a tendency to move further in a positive direction and a negative direction, respectively, when the scan rate is increased from 5 to 100 mV/s. This occurs due to the increased internal resistance of the electrode material when the scanning speed is increased. Anodic and cathodic peak currents gradually shift as the scan rate increases, even though the CV curves remain the same [39].

The charge storage capacity is determined by measuring the galvanostatic charge–discharge (GCD) at different current densities (1 A/g^{-1}). The GCD curves affirmed the pseudocapacitive attitude of the CuS which shows a nonlinear triangle shape. Fig. 6b shows nearly similar triangles indicating electrochemical reversibility throughout charge-discharge periods [40]. Electrochemical impedance spectroscopy (EIS) measurements are conducted to scrutinize the electrochemical efficiency of the electrodes, and the Nyquist plot is shown in Fig. 6c.

The specific capacitances for the CuS at various current densities are shown in Fig. 6e. According to the discharge curve, the specific capacitances are 777.34, 737.60, 683.75, and 651.54 for a current density of 1, 2, 5, and 10 A g^{-1}.

The cycling stability performance of CuS was demonstrated in Fig. 6d. The capacitance retention rate was appraised by charging and discharging over and over 1000 times at a 40 A/g current density. The Ragone plot, which presents an energy density versus power density plot, is shown in Fig. 6f. According to the Ragone plot, the ASC device has a maximum energy density of 40.04 Wh kg^{-1} at 304.5 W kg^{-1} of power density.

A high potential range was obtained by the combination of all materials in the assembled device. As a result of the high potential range the device exhibited high energy density. The device demonstrated a high energy density due to its huge potential range. Moreover, the asymmetric supercapacitor's CV curves were maintained when the scanning rate rose, and relative symmetry was attained without a discernible peak shift, indicating the device's great reaction reversibility (Fig. 7a) [41]. Fig. 7b shows the GCD analysis of the asymmetric device with different currents (between 1 and 10 A) and a voltage window of −1.6–1.5 V. The Nyquist plots of the device were fitted with an equivalent circuit as shown in the inset of Fig. 7c. The specific capacitances for the CuS//WO_3 at various current densities are shown in Fig. 7e. According to the discharge curve, the specific capacitances are 211.43, 141.28, 85.21, and 75.5 F/g at current densities of 1, 2, 5, and 10 A/g, respectively. Specific capacitances gradually decrease with increasing current density. At low current densities, the whole migration of electrolyte ions into the electrode materials is the cause of this phenomenon. Following a series of GCD experiments with a current density of 20A/g, the long-term cycling stability of the ASC device was evaluated (Fig. 7d). The Ragone plot, which presents an energy density versus power density plot, is shown in Fig. 7f. According to the Ragone plot, the ASC device has a maximum energy density of 247.6 Wh kg^{-1} at 1451.7 W kg^{-1} of power density (see Fig. 8).

In order to gain a better understanding of the practical application of CuS//WO3, the schematic of the hybrid supercapacitor (HSC) is provided in Fig. 7a. The assembled CuS//WO_3 was constructed by using WO_3 as the anode and CuS as the cathode, respectively.

A Swagelok cell is frequently used to verify and test the performance of supercapacitors. It is made up of two current collectors and two disc-shaped electrodes that are separated by an electrolyte-soaked separatör [42]. An asymmetric cell with CuS cathode and WO_3 anode was

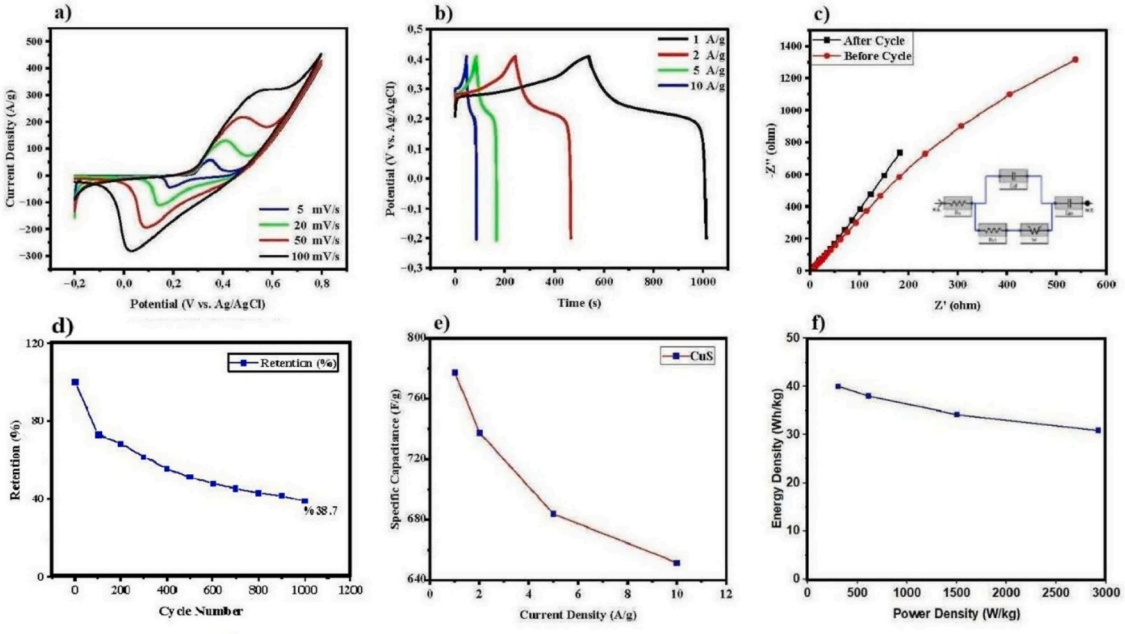


Fig. 6. Electrochemical measurements (a) CV curves of CuS (b) GCD curves of CuS (c) EIS measurement CuS before and after cycles (d) The cycle stability of CuS at 40 A g^{-1} (e) Specific capacitance values as a function of current densities (f) Different Ragone plots of the CuS half cell current densities.

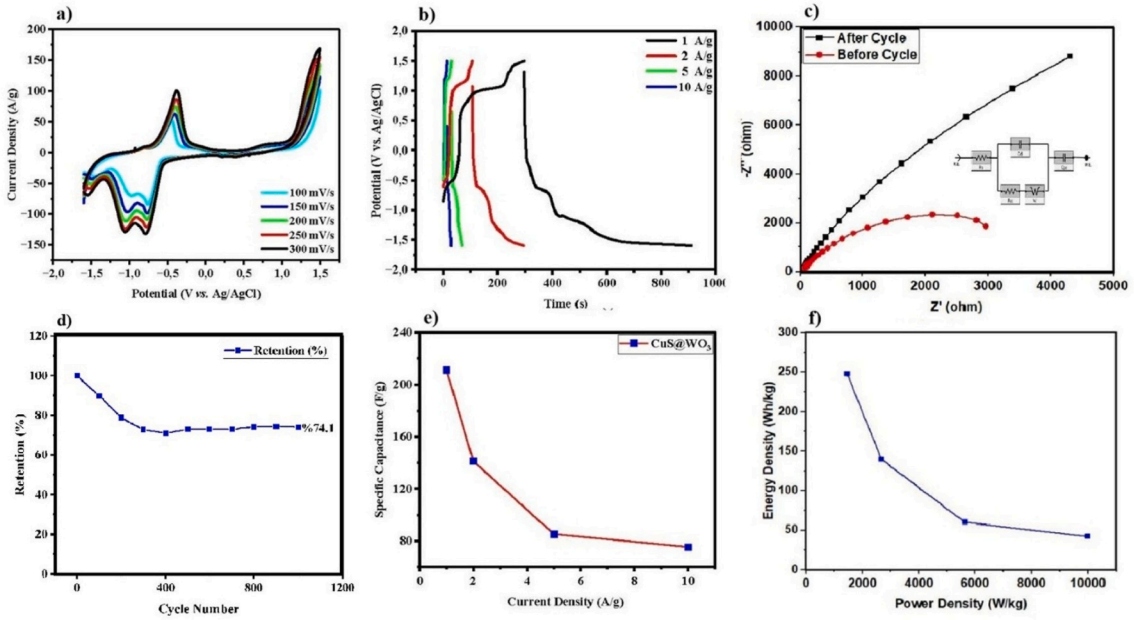


Fig. 7. Electrochemical measurements (a) CV curves of CuS//WO_3. (b) GCD curves of CuS//WO_3. (c) EIS measurement CuS//WO_3 before and after cycles. (d) Specific capacitance values as a function of current densities. (e) The cycle stability of CuS//WO_3 at 20 A g^{-1}. (f) Different Ragone plots of the CuS//WO_3 current densities.

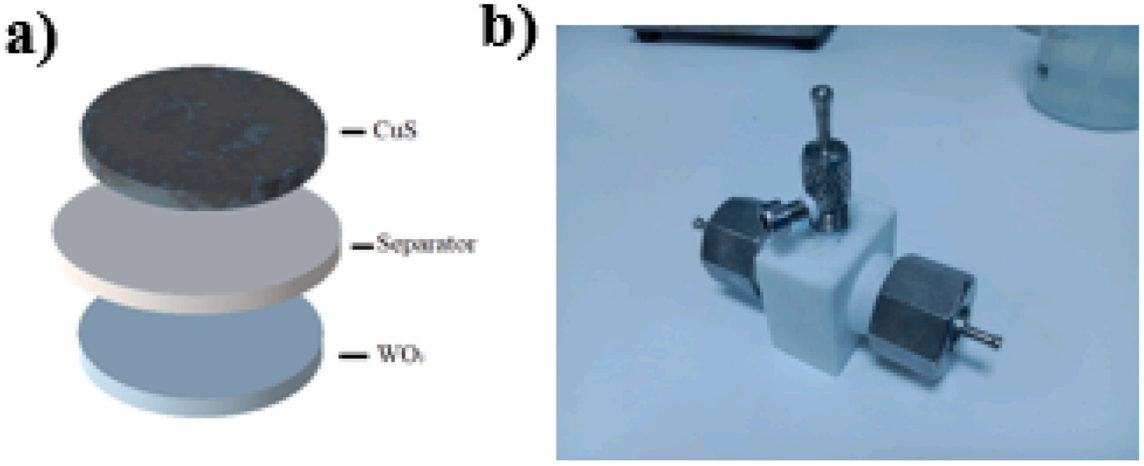


Fig. 8. (a) Schematic representation of the asymmetric device. (b) An image of the asymmetric supercapacitor made from Swagelok cells.

assembled in a Swagelok cell using glass microfiber as the separator (Fig. 7b). The electrochemical performance of the assembled CuS//WO_3 asymmetric supercapacitor was evaluated using the Swagelok cell configuration. The comparative results, summarized in Table 1, demonstrate the specific capacitance values at various current densities (1, 2, 5, and 10 A/g), along with cycling efficiency, energy density, and power density. Notably, the CuS/WO_3 device exhibited a high specific capacitance of 211.43 F/g at 1 A/g, with excellent cycling stability retaining 74.1 % capacitance after 1000 cycles at 40 A/g. Furthermore, the device achieved a superior energy density of 247.6 Wh/kg and a power density of 1.451 kW/kg, significantly outperforming the CuS electrode tested alone. These results highlight the advantageous

Table 1
Electrochemical performance comparison of CuS and CuS/WO_3 electrodes in Swagelok cell and conventional aqueous electrolyte cell.

Electrode Material	Current Density (A/g)	Specific Capacitance (F/g)	Cycling Efficiency (%) (at 40 A/g, 1000 cycles)	Energy Density (Wh/kg)	Power Density
CuS	10	651.54	38.7	40.04	304.5 W/kg
CuS	5	683.75			
CuS	2	737.60			
CuS	1	777.34			
CuS/WO_3 (Swagelok cell)	10	75.5	74.1	247.6	1.451 kW/kg
CuS/WO_3 (Swagelok cell)	5	85.21			
CuS/WO_3 (Swagelok cell)	2	141.28			
CuS/WO_3 (Swagelok cell)	1	211.43			

synergistic effect of combining CuS and WO_3 in the asymmetric configuration, contributing to enhanced energy storage capabilities.

4. Conclusions

In this study, we have demonstrated the design and fabrication of high-performance supercapacitors utilizing asymmetrically designed cathodes and anodes. The supercapacitor system exhibits remarkable performance characteristics, such as the ability to operate at high voltages up to **2.9 V,** with energy densities comparable to those seen in commercially available lithium-ion batteries. This outstanding performance is attributed to the careful selection of materials, with each element complementing the other to optimize energy storage capabilities. Specifically, our supercapacitor showcases an impressive **specific capacitance of 211.43 F/g,** a **high energy density of 247.6 Wh kg−1,** and a **power density of 1.451 kW kg−1** at a current density of **1 A g−1.** These values reflect the excellent electrochemical properties and efficient charge-discharge characteristics of the device. This work paves the way for the development of high-performance, scalable energy storage systems with superior energy and power densities, offering a viable alternative to conventional technologies in high-capacity and rapid charge-discharge applications.

CRediT authorship contribution statement

Irem Ertugrul: Writing – original draft, Visualization, Project administration, Funding acquisition. **Fatma Kilic Dokan:** Writing – review & editing, Writing – original draft, Supervision, Software, Resources, Project administration, Investigation, Conceptualization. **Nuri Burak Kiremitler:** Writing – review & editing, Validation, Supervision, Software, Project administration, Formal analysis. **Mustafa Serdar Onses:** Writing – review & editing, Visualization, Validation, Investigation. **Ertugrul Sahmetlioglu:** Writing – review & editing, Validation, Resources, Investigation, Formal analysis, Conceptualization.

Conflict of interest

The authors have no relevant financial or non-financial interests to disclose.

Acknowledgments

İrem Ertuğrul acknowledges the financial support from Scientific and Technological Research Council of Turkey (2210-C TUBITAK).This work was supported by the Research Fund of the Erciyes University (Project Number FYL-2023-13061).

Data availability

The authors do not have permission to share data.

References

[1] H. Pecenek, F.K. Dokan, M.S. Onses, E. Yılmaz, E. Sahmetlioglu, High energy density hybrid supercapacitors based on graphitic carbon nitride modified BiFeO3 and biomass-derived activated carbon, J. Energy Storage 64 (2023) 107075.
[2] A. Gowdhaman, S.A. Kumar, D. Elumalai, C. Balaji, M. Sabarinathan, R. Ramesh, M. Navaneethan, Ni-MOF derived NiO/Ni/r-GO nanocomposite as a novel electrode material for high-performance asymmetric supercapacitor, J. Energy Storage 61 (2023) 106769.
[3] Yasemin Topal, Senem Tapan, Ersen Gokturk, Ertugrul Sahmetlioglu, Horseradish peroxidase-catalyzed polymerization of *ortho*-imino-phenol: synthesis, characterization, thermal stability and electrochemical properties, J. Saudi Chem. Soc. 21 (6) (September 2017) 731–740.
[4] I. Rathinamala, I.M. Babu, J.J. William, G. Muralidharan, N. Prithivikumaran, CdS microspheres as promising electrode materials for high performance supercapacitors, Mater. Sci. Semicond. Process. 105 (2020) 104677.
[5] S. Xiong, S. Jiang, J. Wang, H. Lin, M. Lin, S. Weng, J. Chen, A high-performance hybrid supercapacitor with NiO derived NiO@ Ni-MOF composite electrodes, Electrochim. Acta 340 (2020) 135956.
[6] W. Sun, L. Xiao, X. Wu, Facile synthesis of NiO nanocubes for photocatalysts and supercapacitor electrodes, J. Alloys Compd. 772 (2019) 465–471.
[7] X. Lu, C. Shen, Z. Zhang, E. Barrios, L. Zhai, Core–shell composite fibers for high-performance flexible supercapacitor electrodes, ACS Appl. Mater. Interfaces 10 (4) (2018) 4041–4049.
[8] C. Li, J. Balamurugan, D.C. Nguyen, N.H. Kim, J.H. Lee, Hierarchical manganese–nickel sulfide nanosheet arrays as an advanced electrode for all-solid-state asymmetric supercapacitors, ACS Appl. Mater. Interfaces 12 (19) (2020) 21505–21514.
[9] C. Li, T. Zhao, X. Feng, S. Liu, L. Li, R. Zha, Z. Zhang, Construction of hierarchical honeycomb-like MnCo2S4 nanosheets as integrated cathodes for hybrid supercapacitors, J. Alloys Compd. 859 (2021) 157815.
[10] S. Yetiman, H. Peçenek, F.K. Dokan, S. Sanduvaç, M. Serdar Onses, E. Yılmaz, E. Sahmetlioglu, Unlocking the potential of bismuth-based materials in supercapacitor technology: a comprehensive review, Chemelectrochem (2024) e202300819.
[11] Z. Ali, M.Z. Iqbal, H.H. Hegazy, Recent advancements in redox-active transition metal sulfides as battery-grade electrode materials for hybrid supercapacitors, J. Energy Storage 73 (2023) 108857.
[12] J. Theerthagiri, R.A. Senthil, P. Nithyadharseni, S.J. Lee, G. Durai, P. Kuppusami, M.Y. Choi, Recent progress and emerging challenges of transition metal sulfides based composite electrodes for electrochemical supercapacitive energy storage, Ceram. Int. 46 (10) (2020) 14317–14345.
[13] M. Hussain, S.D. Alahmari, F.F. Alharbi, S.R. Ejaz, M. Abdullah, S. Aman, H.M. T. Farid, Hydrothermal synthesis of the NiS@ g-C3N4 nanohybrid electrode material for supercapacitor applications, J. Energy Storage 80 (2024) 110289.
[14] S. Rani, L. Bansal, R. Bhatia, R. Kumar, I. Sameera, Engineered nano-architecture for enhanced energy storage capabilities of MoS2/CNT-heterostructures: a potential supercapacitor electrode, J. Energy Storage 84 (2024) 110865.
[15] H. Heydari, S.E. Moosavifard, M. Shahraki, S. ve Elyasi, Facile synthesis of nanoporous CuS nanospheres for high-performance supercapacitor electrodes, energy Chemistry 26 (4) (2017) 762–767.
[16] K.J. Huang, J.Z. Zhang, K. Xing, One-step synthesis of layered CuS/multi-walled carbon nanotube nanocomposites for supercapacitor electrode material with ultrahigh specific capacitance, Electrochim. Acta 149 (2014) 28–33.
[17] Y. Bi, A. Nautiyal, H. Zhang, J. Luo, X. Zhang, One-pot microwave synthesis of NiO/MnO2 composite as a high-performance electrode material for supercapacitors, Electrochim. Acta 260 (2018) 952–958.
[18] S.I. Kim, J.S. Lee, H.J. Ahn, H.K. Song, J.H. Jang, Facile route to an efficient NiO supercapacitor with a three-dimensional nanonetwork morphology, ACS Appl. Mater. Interfaces 5 (5) (2013) 1596–1603.
[19] J.P. Zheng, P.J. Cygan, T.R. Jow, Hydrous ruthenium oxide as an electrode material for electrochemical capacitors, J. Electrochem. Soc. 142 (8) (1995) 2699.
[20] S. Sivakumar, L.N. Prabu, Synthesis and characterization of α-MnO2 nanoparticles for supercapacitor application, Mater. Today Proc. 47 (2021) 52–55.
[21] Y. Zhang, J. Wang, H. Wei, J. Hao, J. Mu, P. Cao, S. Zhao, Hydrothermal synthesis of hierarchical mesoporous NiO nanourchins and their supercapacitor application, Mater. Lett. 162 (2016) 67–70.
[22] S. Yao, F. Qu, G. Wang, X. Wu, Facile hydrothermal synthesis of WO3 nanorods for photocatalysts and supercapacitors, J. Alloys Compd. 724 (2017) 695–702.
[23] E. Turaç, M. Ak, E. Şahmetlioglu, M. Kasım Şener, M.A. Kaya, Synthesis and characterization of poly {2-[3-(1 H-pyrrol-2-yl) phenyl]-1 H-pyrrole} and its copolymer with EDOT, Russ. J. Gen. Chem. 81 (2011) 2510–2516.
[24] A. Kumbul, E. Gokturk, E. Turaç, E. Sahmetlioglu, Enzymatic oxidative polymerization of *para*-imine functionalized phenol catalyzed by horseradish peroxidase, Polym. Adv. Technol. 26 (9 Sep) (2015) 1047–1197.
[25] E. Turac, E. Sahmetlioglu, L. Toppare, H. Yuruk, Synthesis, characterization and optoelectrochemical properties of poly (2, 5-di (thiophen-2-yl-) 1-(4-(thiophen-3-yl) phenyl)-1H-pyrrole-co-EDOT), Des. Monomers Polym. 13 (3) (2010) 261–275.
[26] S. Saini, P. Chand, Effect of aqueous electrolytes on h-WO3 nanorods as an electrode material for supercapacitor application, Chem. Phys. Lett. 802 (2022) 139760.
[27] S.M. AL-Jawad, A.A. Taha, A.M. Redha, Studying the structural, morphological, and optical properties of CuS: ni nanostructure prepared by a hydrothermal method for biological activity, J. Sol. Gel Sci. Technol. 91 (2019) 310–323.
[28] D.K. Kulurumotlakatla, G. Saeed, D. Lee, R. Vinodh, S. Ansar, B. Tadesse, M. C. Kang, Integrating 0D Cu3Fe4 (PO4) 6 nanoparticles as anode and triangular-shaped ZnMoO4 nanorods as cathode materials for enriched redox contributions of asymmetric supercapacitor, J. Energy Storage 101 (2024) 113803.
[29] Y.H. Li, M.Y. Qi, Z.R. Tang, Y.J. Xu, Coupling organic synthesis and hydrogen evolution over composite WO3/ZnIn2S4 Z-scheme photocatalyst, J. Phys. Chem. C 126 (4) (2022) 1872–1880.
[30] P.A. Shinde, A.C. Lokhande, A.M. Patil, C.D. Lokhande, Facile synthesis of self-assembled WO3 nanorods for high-performance electrochemical capacitor, J. Alloys Compd. 770 (2019) 1130–1137.
[31] Hsu. Yu-Kuei, et al., Synthesis of copper sulfide nanowire arrays for high-performance supercapacitors, Electrochim. Acta 139 (1 September 2014) 401–407.
[32] Susmi Anna Thomas, et al., A comprehensive review on tungsten oxide nanostructures-based electrochromic supercapacitors and machinelearning models for design and process parameter optimization, Energy storage 5 (2023) 8.
[33] Dong. Xu, et al., Nanostructured tungsten oxide as photochromic material for smart devices, energy conversion, and environmental remediation, J. Photochem. Photobiol. C Photochem. Rev. 53 (2022) 100555.
[34] A. Ishfak, An-Nafe A brief review on applications of tungsten oxide nanoparticles, J. Med. Nanomater. Chem. 7 (2025) 216–235.

[35] Majumdar Dipanwita, Recent progress in copper sulfide based nanomaterials for high energy supercapacitor applications, J. Electroanal. Chem. 880 (2021) 114825.
[36] Tehrani. Shariatmadar, et al., Hydrothermal synthesis and characterization of WO3 nanostructures: effect of reaction time, Mater. Res. Express 7 (2020), 015911.37. Xu.
[37] Wence, et al., Synthesis and properties of morphology controllable copper sulphide nanosheets for supercapacitor application, Electrochim. Acta 211 (2016) 891–899.
[38] M.O. Yanik, E.A. Yigit, Y.E. Akansu, E. Sahmetlioglu, Magnetic conductive polymer-graphene nanocomposites based supercapacitors for energy storage, Energy 138 (2017) 883–889, https://doi.org/10.1016/j.energy.2017.07.022.
[39] Y. Wang, Y. Liu, H. Wang, W. Liu, Y. Li, J. Zhang, J. Yang, Ultrathin NiCo-MOF nanosheets for high-performance supercapacitor electrodes, ACS Appl. Energy Mater. (2019), https://doi.org/10.1021/acsaem.8b02128.
[40] H. Wang, M. Liang, D. Duan, W. Shi, Y. Song, Z. Sun, Rose-like Ni3S4 as batterytype electrode for hybrid supercapacitor with excellent charge storage performance, Chem. Eng. J. 350 (2018) 523–533, https://doi.org/10.1016/j.cej.2018.05.004.
[41] J. Xu, Z. Meng, Z. Hao, X. Sun, H. Nan, H. Liu, X. Hu, Oxygen-vacancy abundant alpha bismuth oxide with enhanced cycle stability for high-energy hybrid supercapacitor electrodes, J. Colloid Interface Sci. 609 (2022) 878–889.
[42] D. Bhattacharjya, D. Carriazo, J. Ajuria, A. Villaverde, Study of electrode processing and cell assembly for the optimized performance of supercapacitor in pouch cell configuration, J. Power Sources 439 (2019) 227106.